

# LOW POWER 3-AXIS LORENTZ FORCE NAVIGATION MAGNETOMETER

M.J. Thompson, M. Li, and D.A. Horsley

University of California, Davis, USA

## ABSTRACT

Demonstrated here is a MEMS magnetometer fabricated with the ST Microelectronics THELMA process that uses a single MEMS structure to detect magnetic flux in two axes. The device is comprised of a single Lorentz force actuator where the resulting shuttle motion is detected in two axes using differential in-plane capacitive sensing electrodes and a single-ended out-of-plane electrode. Three axis magnetic flux sensing is achieved using two perpendicular structures on the same die. The device is intended for electronic compass navigation applications and using a total of 300  $\mu\text{W}$  of drive power has a 3-axis angular resolution of 0.8 degrees/rt-Hz in California, USA.

## INTRODUCTION

There is a growing interest in three-axis magnetic field sensors for low-cost, low-power applications such as electronic compasses for smart mobile phones. In these applications, Lorentz force magnetometers are advantageous over other magnetic sensors because they are constructed using the same fabrication process as MEMS inertial sensors such as gyroscopes and accelerometers currently used in mobile phones and consumer electronics. Previous MEMS magnetometers were designed to detect Lorentz force in a single axis, requiring three MEMS structures to produce a three-axis sensor suitable for use as an electronic compass [1]. Here the magnetometer is comprised of two MEMS structures that each measure magnetic flux in two axes.

## DESIGN

The 225  $\mu\text{m}$  by 1000  $\mu\text{m}$  magnetometer structure, shown in Fig. 1, is fabricated in the ST Microelectronics ThELMA process and is vacuum encapsulated at the chip level. The MEMS structure is fabricated from a 15  $\mu\text{m}$  thick layer of epitaxial polysilicon while a thin buried polysilicon layer forms the interconnect and the Z-axis capacitive sensing electrode beneath the MEMS structure. The device is a resonant sensor with current-carrying flexures that in a magnetic field apply Lorentz force to a MEMS shuttle. The direction of the Lorentz force applied to the MEMS shuttle is perpendicular to the current and perpendicular to the magnetic flux as shown in (1a, 1b)

$$F_x = (i_{AC} l_{eff})_y \times B_z \quad (1a)$$

$$F_z = -(i_{AC} l_{eff})_y \times B_x \quad (1b)$$

where  $i_{AC}$  is an AC current,  $l_{eff}$  is the effective length of the beam,  $B$  is the magnetic field and the subscripts  $x$ ,  $y$ ,  $z$  represent direction.

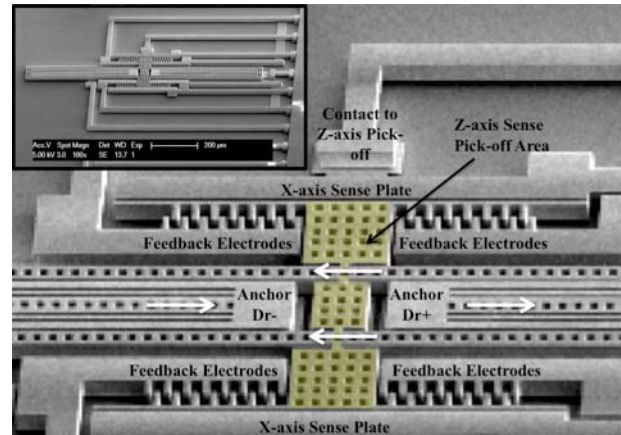


Fig. 1: SEM image of a magnetometer structure. White arrows indicate the current flow through the flexures while the location of the lower sensing electrode is indicated in yellow. The actual device tested here had two pairs of parallel plate electrodes rather than the combination of parallel-plate and comb-finger electrodes shown in the SEM.

This magnetometer is designed to allow the MEMS shuttle to move in two axes so that the motion from the two axes of magnetic field is detectable. The two directions have the same shuttle mass but have different stiffness and the in-plane and out-of-plane modes are shown in Fig. 2.

In electronic compass applications, the field signal  $B(t)$  is slowly varying with a bandwidth of a few Hertz. To maximize the force sensitivity, the Lorentz force signal is modulated at the MEMS structure's natural frequency by the flexure current,  $i(t) = i_{AC} \sin(\omega_n t)$ . For each axis, the motion of the magnetometer ( $x$ ) with a Lorentz force ( $F$ ) applied at the natural frequency is described by (2)

$$\ddot{x} + \frac{\omega_n}{Q} \dot{x} + \omega_n^2 x = -\frac{F}{m} \sin(\omega_n t) \quad (2)$$

where  $x$  is the displacement,  $\omega_n$  is the natural frequency,  $F$  is the applied Lorentz force in (1a or 1b),  $Q$  is the quality factor and  $m$  is the mass. When  $B(t)$  is slowly varying in comparison to  $\omega_n$ , the solution to (2) can be described by (3) where the solution is separated in time by slow time, ( $\eta = \omega_n t / Q$ ), and stretched time ( $\omega_n t$ ). Here  $x_c$  and  $x_s$  are the components which represent the slow time dynamics of the output at the drive frequency,

$$x = x_c(\eta) \cos(\omega_n t) + x_s(\eta) \sin(\omega_n t) \quad (3)$$

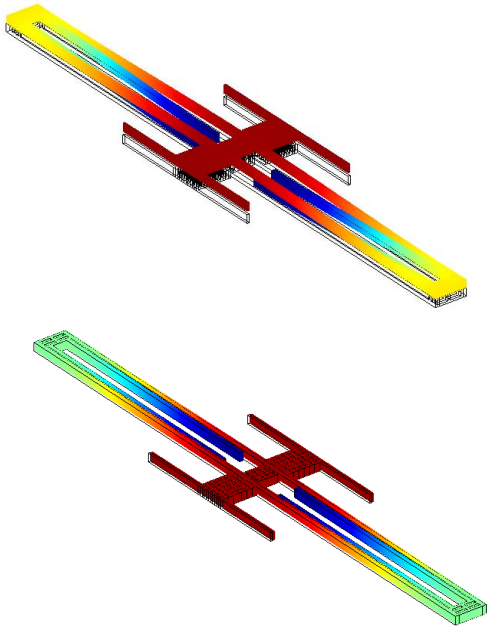


Fig. 2: FEM modeshapes for the out-of-plane (top) and in-plane (bottom) modes simulated using COMSOL software.

Averaging methods are used to solve for  $x_c$  and  $x_s$  and the solution is given by (4a, 4b) described in the Laplace domain [2],

$$\frac{X_c(s)}{F} = \frac{2\pi f_n}{k \left( s + \frac{2\pi f_n}{Q} \right)} \quad (4a)$$

$$\frac{X_s(s)}{F} = 0 \quad (4b)$$

where  $f_n = \omega_n/2\pi$  is the natural frequency in Hz.

The motion signal is demodulated by multiplication with a sinusoid at  $f_n$ . Equation (4a), which describes a first order system with a -3dB bandwidth of  $f_n/Q$ , represents the dynamics of the demodulated motion signal. Note that the low-frequency force-to-displacement gain of (4a) is  $Q/k$ . Each mode will have a different  $f_n$ ,  $k$  and  $Q$  and the demodulated value is described by (4a) with these values.

The operation of the sensor is depicted in Fig. 3. The flexure current is modulated through the Lorentz beam at both modal frequencies so that Lorentz forces are applied to the MEMS shuttle at the two modal frequencies. The in-plane mode is excited when magnetic field is present in the Z-axis and current is modulated through the flexures near the in-plane modal frequency ( $f_x$ ) of 20.3 kHz. Similarly, the out-of-plane mode is excited by X-axis field and current that is modulated near the out-of-plane modal frequency ( $f_z$ ) of 47 kHz. Measurement of field in the second in-plane (Y) axis is performed using a second structure rotated by 90° relative to the first structure. On each magnetometer, the in-plane motion of the MEMS shuttle is measured with two differential parallel-plate capacitors and the out-of-plane motion is measured with a single-sided bottom electrode.

Capacitive sensing is performed using a source-follower JFET amplifier on each of the two in-plane electrodes as well as the out-of-plane electrode. The output of the in-plane sensing amplifier is demodulated at the in-plane frequency ( $f_x$ ) and the output of the out-of-plane amplifier is demodulated at the out-of-plane frequency ( $f_z$ ). The resulting displacement at each mode is amplified by the quality factor  $Q$ , which is 5000 for the out-of-plane mode and 1500 for the in-plane mode.

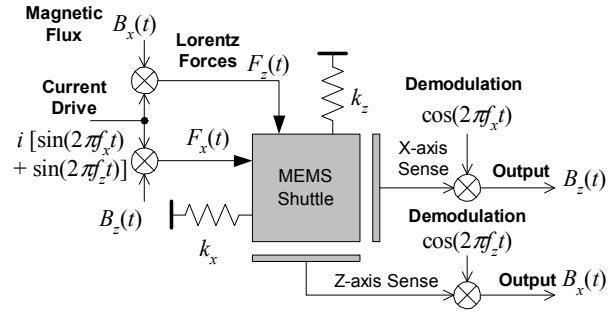


Fig. 3: Sensor block-diagram. Sinusoidal currents at two frequencies modulate the low-frequency field signals ( $B_x$ ,  $B_z$ ) to produce forces centered around the in-plane and out-of-plane natural frequencies ( $f_x$ ,  $f_z$ ).

## EXPERIMENTAL RESULTS

### Modal Frequencies

The magnitude frequency response of the sensor at each of the two modal frequencies is shown in Fig. 4 and Fig. 5. Fig. 4 shows the frequency spectrum for the out-of-plane motion showing the first modal frequency at 46.98 kHz. The response is shown for different input force amplitudes to illustrate the nonlinear Duffing behavior that occurs at large displacement amplitudes. This behavior is caused by the parallel plate capacitor nonlinearity, which causes spring softening.

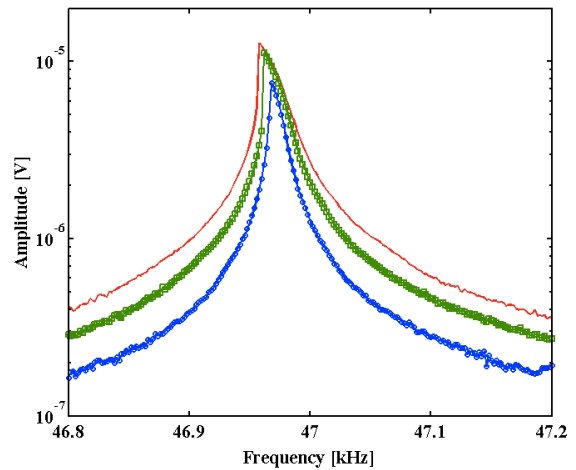


Fig. 4: Frequency spectrum of the out-of-plane mode for different input force amplitudes.

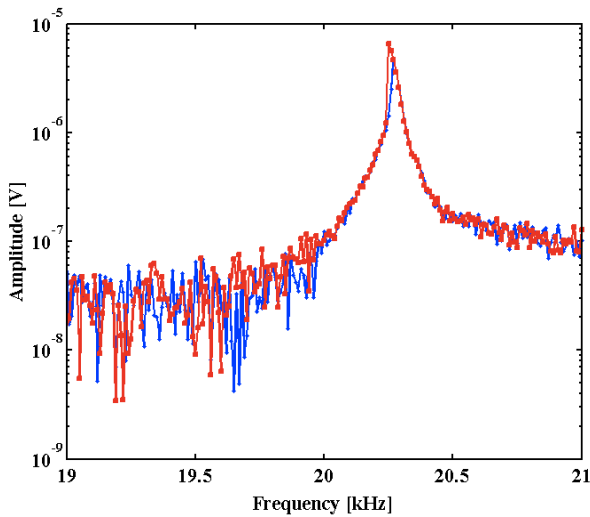


Fig. 5: Frequency spectrum of the in-plane mode.

Fig. 5 shows the frequency response for in-plane motion. The in-plane natural frequency is 20.3 kHz. The experimentally-measured frequencies compare favorably to the frequencies predicted by the FEM model, which were 25.9 kHz and 54.1 kHz for the in-plane and out-of-plane modes, respectively. The difference between the FEM results and the experiment are attributable to the reduction in line-width that occurs during device fabrication.

### Frequency Response

To measure the response of the magnetometer to magnetic field, the sensor was placed on an electromagnet. The frequency response of the sensor was measured by applying AC magnetic fields from 2 Hz to 100 Hz in 1 Hz increments. The outputs of the in-plane and out-of-plane motion sensing amplifiers were demodulated at the flexure current excitation frequencies (nominally 20.3 kHz and 47 kHz for the in-plane and out-of-plane modes, respectively) using a lock-in amplifier (HF2LI, Zurich Instruments Inc.). To minimize the effect of variations in the modal frequencies due to changes in temperature and supply voltages, measurements were collected with the excitation/demodulation frequency at various frequency offsets from the nominal frequency of the in-plane and out-of-plane modes. Fig. 6 shows the demodulated response of the magnetometer for a 290  $\mu\text{T}$  X-axis input field. The output response peaks at -85 dBV for a 7 Hz magnetic input. Fig. 7 shows the demodulated response of the magnetometer for a 1.9 mT Z-axis input field. The magnetometer has a maximum response of -70.8 dBV at 2 Hz. The measured 3 dB bandwidth is approximately equal to  $f_n/Q$  and  $f_n/Q$  for each axis. Fig. 6 and Fig. 7 show the measured noise floor of the sensor in each axis, which corresponds to an X-axis magnetic field resolution of 296 nT/rt-Hz and a 137 nT/rt-Hz resolution for Z-axis field. The resolution, which is limited by electronic noise, translates to an angular resolution in three axes of 0.8 deg/rt-Hz in California, USA

(35  $\mu\text{T}$  Earth's magnetic field). In comparison, the theoretical Brownian noise limited resolution of the three axes is 133 nT/rt-Hz for the Z-axis resolution and 111 nT/rt-Hz for the X and Y axis resolution, which translates to an angular resolution in 3-axes of 0.52 deg/rt-Hz. To achieve Brownian limited resolution, the relative amplitude of the electronic noise must be reduced tenfold for the X and Y axis by either increasing the DC bias voltage used for sensing, reducing the parasitic capacitance on the sensing electrodes, or by parametrically-amplifying the mechanical gain of the MEMS structure [3,4].

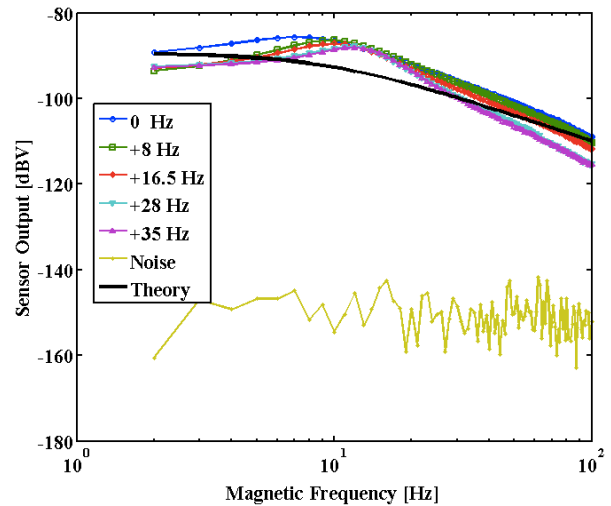


Fig. 6: Response to a 290  $\mu\text{T}$  X-axis AC magnetic field input. Measurements are shown with the flexure current frequency at various offsets from the 47 kHz out-of-plane fundamental modal frequency. The noise floor is -150 dBV and the sensor bandwidth is approximately 10 Hz.

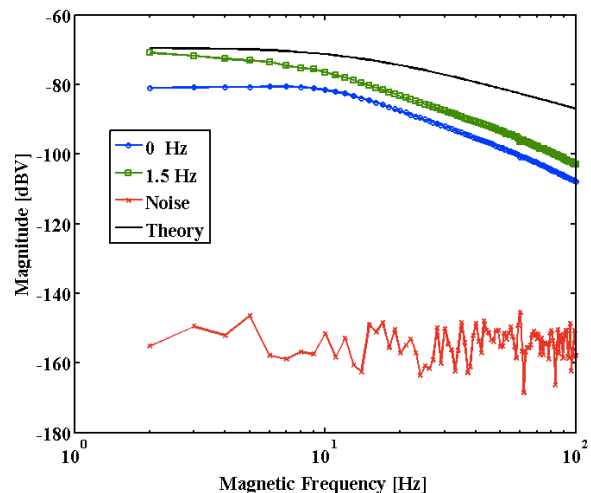


Fig. 7: Response to a 1.9 mT Z-axis AC magnetic field input. Measurements are shown with the flexure current frequency offset from the 20.36 kHz in-plane fundamental modal frequency. The measured noise floor is -153.7 dBV and the sensor bandwidth is approximately 13 Hz.

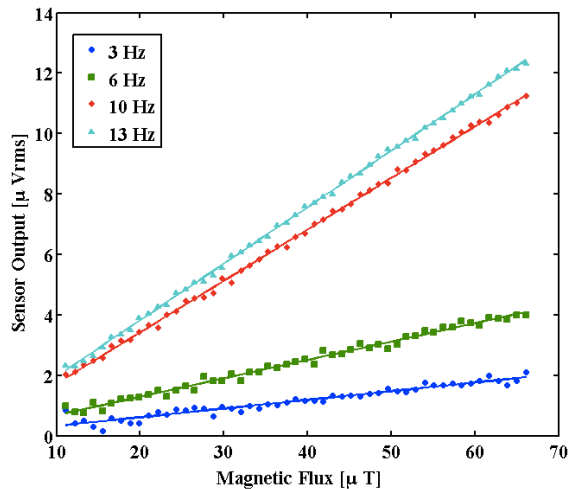


Fig. 8: X-axis magnetic field transfer characteristic measured with AC magnetic flux inputs at various frequencies.

### Linearity Experiments

The magnetic field transfer characteristic of the sensor was measured by sweeping the amplitude of the applied magnetic field from 1  $\mu\text{T}$  to 68  $\mu\text{T}$  and recording the demodulated voltage amplitude. The measured transfer characteristics for X and Z axis fields are shown in Fig. 8 and Fig. 9, respectively. In Fig. 8, it is clear that the response at 10 Hz and 13 Hz is greater than the response at 3 Hz and 6 Hz. This result matches the frequency response measurement shown in Fig. 6. This unusual response is attributed to nonlinear spring-softening Duffing behavior, which is shown in Fig. 5. The maximum X-axis field sensitivity shown at 13 Hz is  $0.186 \text{ V}_{\text{rms}}/\text{T}$ . As shown in Fig. 9, the response to Z-axis field at 3 Hz, 4 Hz and 5 Hz is very similar which is supported by the frequency response measurement shown in Fig. 7. For Z-axis field, the sensitivity is  $0.17 \text{ V}_{\text{rms}}/\text{T}$ .

### CONCLUSIONS

Here we demonstrate a two-axis magnetic sensor based on a single MEMS structure. The sensor's magnetic field resolution is limited by electronic noise from the detection electronics. With 300  $\mu\text{W}$  power used for flexure current, the sensor has a 3-axis angular resolution of 0.8 degrees/rt-Hz in California, USA. However, improvements in the detection electronics are expected to yield Brownian noise-limited resolution of 0.52 degrees/rt-Hz. The sensitivity for out-of-plane magnetic flux inputs is  $0.17 \text{ V}_{\text{rms}}/\text{T}$ . The sensing mode for in-plane magnetic flux inputs exhibits nonlinear behavior, which causes the maximum sensitivity to peak at 13 Hz with a sensitivity of  $0.186 \text{ V}_{\text{rms}}/\text{T}$ . The relatively high natural frequencies of the structure make the sensor less sensitive to acceleration. Additionally, the sensitivity to low-frequency inertial forces is orders of magnitude lower than the sensitivity to the Lorentz force, which is amplified by the device's  $Q$ .

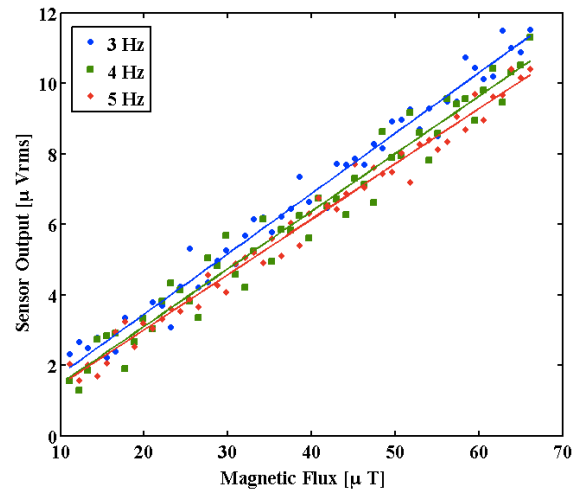


Fig. 9: Z-axis magnetic field transfer characteristic measured with AC magnetic flux inputs at various frequencies.

### ACKNOWLEDGEMENTS

This work is supported by NSF CAREER award CMMI-0846379. M. Li's work at UC Davis was conducted under the Global Research Experience in Advanced Technologies (GREAT) Program. The authors gratefully acknowledge B. Vigna, S. Zerbini, and E. Lasalandra at ST Microelectronics for device fabrication.

### REFERENCES

- [1] J. Kynäräinen, J. Saarilahti, H. Kattelus, A. Kärkkäinen, T. Meinander, A. Oja, P. Pekko, H. Seppä, M. Suhonen, and H. Kuisma, "A 3D micromechanical compass," *Sens. Actuators A*, vol. 142, pp. 561-568, Apr. 2008.
- [2] A. H. Nayfeh and D. T. Mook, *Nonlinear Oscillations*, Wiley-Interscience, New York, 1995.
- [3] M. J. Thompson and D. A. Horsley, "Lorentz force MEMS magnetometer," in *2010 Solid-State Sens. Actuators, Microsyst. Workshop*, Hilton Head, SC, June 6-10, 2010, pp. 44-48.
- [4] M.J. Thompson and D.A. Horsley, "Parametrically-amplified MEMS magnetometer," *Proc. 15th Int. Conf. Solid-State Sensors Actuators & Microsystems (Transducers 2009)*, Denver, CO, June 21-25, 2009, pp. 1194-1197.